J. KSIAM Vol.20, No.1, 37–50, 2016 http://dx.doi.org/10.12941/jksiam.2016.20.037

LARGE EDDY SIMULATION OF TURBULENT CHANNEL FLOW USING ALGEBRAIC WALL MODEL

MUHAMMAD SAIFUL ISLAM MALLIK[1,2†] AND MD. ASHRAF UDDIN[1]

[1] DEPARTMENT OF MATHEMATICS, SHAHJALAL UNIVERSITY OF SCIENCE & TECHNOLOGY, BANGLADESH
E-mail address: auddin-mat@sust.edu

[2] DEPARTMENT OF ARTS AND SCIENCES, AHSANULLAH UNIVERSITY OF SCIENCE & TECHNOLOGY, BANGLADESH
E-mail address: saiful1185@yahoo.com

ABSTRACT. A large eddy simulation (LES) of a turbulent channel flow is performed by using the third order low-storage Runge–Kutta method in time and second order finite difference formulation in space with staggered grid at a Reynolds number, $Re_\tau = 590$ based on the channel half width, δ and wall shear velocity, u_τ. To reduce the calculation cost of LES, algebraic wall model (AWM) is applied to approximate the near-wall region. The computation is performed in a domain of $2\pi\delta \times 2\delta \times \pi\delta$ with $32 \times 20 \times 32$ grid points. Standard Smagorinsky model is used for subgrid-scale (SGS) modeling. Essential turbulence statistics of the flow field are computed and compared with Direct Numerical Simulation (DNS) data and LES data using no wall model. Agreements as well as discrepancies are discussed. The flow structures in the computed flow field have also been discussed and compared with LES data using no wall model.

1. INTRODUCTION

Turbulent channel flow is an important test case for numerical simulations and validation of turbulent models. It is commonly encountered in engineering practice. Because of the simplicity in geometry and its wide application background in industry, the experimental and computational studies of the turbulent channel flow have been carried out extensively [1-9].

In recent years, with the development of the technique of numerical simulation, LES has been demonstrated to be an useful research tool for understanding the physics of turbulence in more complex geometries than DNS. Although DNS is considered as the exact approach to turbulence simulation, yet it is very expensive if the flow Reynolds number is very high and computational grid is very large. LES is a method in which large-scale motions are exactly calculated and the SGS motion is modeled [5-6].

Received by the editors December 21 2015; Revised March 3 2016; Accepted in revised form March 3 2016; Published online March 23 2016.

2000 *Mathematics Subject Classification.* 76F65.

Key words and phrases. Large Eddy simulation, Turbulent channel flow, Algebraic wall model.

† Corresponding author.

To conduct LES in wall bounded turbulent flows [3-10], a large number of computational nodes are generally required to resolve the boundary layers. Wall integration of turbulence models requires the first computational node above the wall to be situated within the viscous sublayer. But, wall functions do not require the excessive grids in the boundary layer. For instance, the first computational node might be positioned in the logarithmic inertial layer, which will lead to a significant reduction in the number of computational nodes in the boundary layer [11]. But, this is to be done without a significant loss in accuracy. However, the computational cost of LES can be reduced by using wall stress models.

Wall stress models provide an algebraic relationship between local wall shear stresses and tangential velocities at the wall-nearest velocity nodes. This approach was first employed by Schumann [12] for performing a plane channel flow simulation. He assumed that the streamwise and spanwise velocity fluctuations are in phase with the respective surface shear stress components. A number of improvements to Schumann's model were suggested by, for example, GrÖtzbach [8] and Werner and Wengle [9], who wanted to avoid having to know the mean wall shear stress *a priori* and to simplify the computations. Another wall model was proposed by Piomelli *et al.* [13] as a modification of the previous wall models to empirically account for the effect of sweep and ejection events on the wall shear stress. To reduce the calculation cost of LES, in this study we have used AWM [14] at the near wall region.

To perform LES in turbulence, discretization method is another concern. For spatial discretization the conventional finite difference method is widely used with structured grids [15-17], and for temporal discretization the explicit Runge–Kutta methods [18-19] are a popular choice. Although in explicit Runge–Kutta methods generally the Poisson equation is solved for the pressure at each stage, but these methods generally have better stability properties, do not have a start-up problem, and easily allow for adaptive time stepping [19].

To conduct LES in a turbulent channel flow it is necessary to do long time integration that need much wider computation region. In this case, the application of a low-storage Runge–Kutta scheme is significant to make sufficient utilization of computer resources. Because, low-storage Runge–Kutta schemes require minimum levels of memory locations during the time integration and efficiently comply with the modern large-scale scientific computing needs. A number of third-order low-storage explicit Runge–Kutta schemes were derived by Williamson [20].

The objective of this study is to perform LES of a plane turbulent channel flow using AWM. Spatial and temporal discretization has been done by using the second order finite difference formulation and third order low-storage explicit Runge–Kutta method respectively in a staggered grid system. For SGS modeling the Standard Smagorinsky model has been used. Essential turbulence statistics of the computed flow field are investigated and compared with DNS data of Moser *et al*. [2] and LES data of Uddin and Mallik [5]. Instantaneous streamwise velocity distribution at the centerline plane of the channel and instantaneous streamwise shear velocity distribution at the immediate vicinity of the wall have also been discussed by different contour plots and compared with those obtained by Uddin and Mallik [5]. Vortical structures using second invariant of velocity gradient tensor in the turbulent flow field are visualized and compared with that of Uddin and Mallik [5]. More specifically, the prime objective of our

investigation is whether our simulation is able to capture turbulence at low resolution by using AWM in LES.

2. GOVERNING EQUATIONS

The governing equations of LES for an incompressible plane turbulent channel flow are the filtered Navier–Stokes and continuity equations for constant density in Cartesian co-ordinates given as [5, 21]:

$$\frac{\partial \bar{u}_i}{\partial t} + \frac{\partial}{\partial x_j}\left(\bar{u}_i\,\bar{u}_j + \tau_{ij}\right) = -\frac{1}{\rho}\frac{\partial \bar{p}}{\partial x_i} + \frac{\partial}{\partial x_j}\left[\nu\left(\frac{\partial \bar{u}_i}{\partial x_j} + \frac{\partial \bar{u}_j}{\partial x_i}\right)\right], \tag{2.1}$$

$$\frac{\partial \bar{u}_i}{\partial x_i} = 0 \tag{2.2}$$

where the index $i, j = 1, 2, 3$ refers to the x, y and z directions respectively. Here $\bar{u}_x$, $\bar{u}_y$, $\bar{u}_z$ are streamwise, wall normal and spanwise filtered velocity respectively. $\bar{p}$ is the filtered pressure, ρ represents the density of the fluid and ν is the kinematic viscosity. τ_{ij} is SGS Reynolds stress which is in fact the large scale momentum flux caused by the action of the small or unresolved scales. The equations are non-dimensioned by the channel half-width δ, and the wall shear velocity u_τ. The flow Reynolds number is therefore written as $Re_\tau = u_\tau \delta/\nu$. A schematic geometry of the plane turbulent channel flow and the co-ordinate system are shown in Fig. 1.

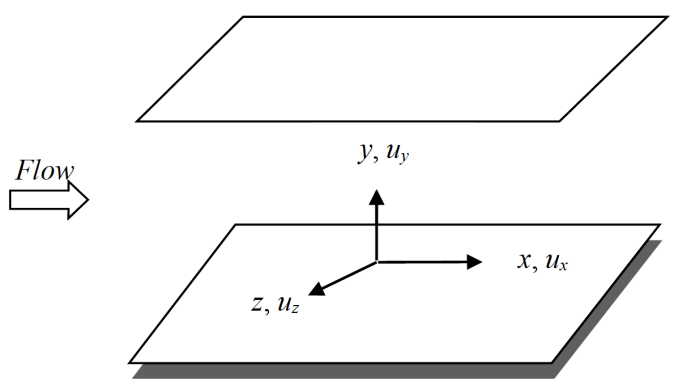

FIGURE 1. Schematic geometry of plane channel flow.

In LES, the velocity field u_i is decomposed into a filtered or large scale component $\bar{u}_i$ and a SGS component u'_i by applying a spatial filtering operation. This decomposition is represented as [21]:

$$u_i = \bar{u}_i + u'_i \tag{2.3}$$

The resolved velocity component, $\bar{u}_i$ can be expressed as

$$\bar{u}_i\left(x_1,\, x_2,\, x_3,\, t\right) = \int_{-\infty}^{+\infty}\int_{-\infty}^{+\infty}\int_{-\infty}^{+\infty}\left(\prod_{i=1}^{3} G_i\left(x_i - x_i'\right)\right) u_i\left(x_1',\, x_2',\, x_3',\, t\right)\, dx_1'\, dx_2'\, dx_3' \quad (2.4)$$

where $G_i\left(x_i - x_i'\right)$ is a general filtering function which satisfies the following relation:

$$\int_{-\infty}^{+\infty}\int_{-\infty}^{+\infty}\int_{-\infty}^{+\infty}\left(\prod_{i=1}^{3} G_i\left(x_i - x_i'\right)\right) dx_1'\, dx_2'\, dx_3' = 1 \quad (2.5)$$

The SGS flow field, u'_i is obtained by subtracting the filtered field from the full field. The effect of the SGS field appears through the SGS Reynolds stress term, which is defined as

$$\tau_{ij} = \overline{u_i\, u_j} - \bar{u}_i\, \bar{u}_j. \quad (2.6)$$

LES requires a model to represent the effects of the SGS field on the filtered field. The models used to approximate the SGS Reynolds stress are called SGS models. The simplest and most popular SGS model is the Standard Smagorinsky model. In this model, τ_{ij} is computed as [21]:

$$\tau_{ij} = -\,2\,\nu_S \bar{S}_{ij} \quad (2.7)$$

where,

$$\nu_s = \left(C_S\,\Delta\right)^2\,\left|\bar{S}\right| \quad (2.8)$$

is the SGS eddy viscosity The quantity C_S is the Smagorinsky constant which is not fixed. Many authors used different values of C_S for LES in turbulent channel flows. In this study, the computation is performed for $C_S = 0.065$ for a channel flow [3]. $\Delta = \left(\Delta x\,\Delta y\,\Delta z\right)^{1/3}$ is filter width and $\left|\bar{S}\right| = \sqrt{2\,\bar{S}_{ij}\,\bar{S}_{ij}}$ is the magnitude of strain rate, where $\bar{S}_{ij} = \frac{1}{2}\left(\frac{\partial\,\bar{u}_i}{\partial\,x_j} + \frac{\partial\,\bar{u}_j}{\partial\,x_i}\right)$.

For the reduced growth of the small scales at the near wall region the SGS eddy viscosity can be modified as [5, 6]:

$$\nu_s = \left(C_S f_S\,\Delta\right)^2\,\left|\bar{S}\right| \quad (2.9)$$

Here $f_S = 1 - \exp\left(-\frac{y^+}{A^+}\right)$ is the Van-Driest damping function, where y^+ is the distance from the wall in viscous wall units defined as $y^+ = \frac{y\,u_\tau}{\nu}$ and A^+ is a constant usually taken to be approximately 25 [21].

3. Numerical methods and grid system

The governing equations of LES are solved using the third order low-storage explicit Runge–Kutta method in time [22] and the second order finite difference formulae in space. The coupling between continuity equation and pressure fields is performed by the simplified marker-and-cell (SMAC) method [23]. Poisson equation is solved iteratively by Incomplete Cholesky Decomposition Conjugated Gradient method. The Spalding equation is solved by iterative procedure based on the Newton method.

Conventional numerical algorithms based on a structured computational grid mostly fall into three classes: regular, staggered, and collocated grid systems. In this study, the staggered

grid system has been used.Staggered grids may be constructed by several methods. On the staggered grid, scalar variable pressure are stored at the nodes and velocities are stored at the middle of the two nodes. A staggered grid system in a two-dimensional plane has been given in our previous papers [5, 6]. The biggest advantage of the staggered arrangement is the strong coupling between the velocities and the pressure.

When the computational domain is discretized by the grid points, the governing equations should be discretized in this domain. This will result in a set of ordinary differential equations for each grid point in space. There are different methods to discretize the equations and the finite difference method is the most straightforward one. Finite difference method is simply the substitution of the continuous differential operators with corresponding discrete operators. There are a variety of discretization techniques available for developing discrete approximations to a set of governing partial differential equations such as Navier–Stokes equations. Let the finite difference operator with stencil size 1 acting on a discrete variable φ with respect to x for structural Cartesian meshes with uniform spacing be defined as [5, 6]:

$$\frac{\partial_1 \varphi}{\partial_1 x}\Big|_{i,\,j,\,k} = \frac{\varphi_{i,\,j,\,k} - \varphi_{i-1,\,j,\,k}}{\Delta x} \tag{3.1}$$

where the grid spacings Δx are constant in x direction, and $(i,\ j,\ k)$ denotes associated mesh indices in x, y and z directions. Discrete operators in the y and z directions are similarly defined. In addition to the discrete differencing operator we also define interpolation operators given in our previous papers [5, 6].

Since the Navier–Stokes equations are unsteady, to solve them numerically both spatial and temporal discretizations are needed. For temporal discretization a low-storage explicit Runge–Kutta method is shortly described by Uddin and Mallik [5], and Mallik *et al.* [6]. Such a scheme requires only two levels of memory locations during the time integration.

4. COMPUTATIONAL PARAMETERS

The computational domain of the mesh is selected to be $2\,\pi\,\delta \times 2\,\delta \times \pi\,\delta$ in streamwise, wall normal and spanwise directions respectively. The computation is performed using $32 \times 20 \times 32$ grid points in the corresponding directions, and the possible Reynolds number is $Re_\tau = 590$ based on the channel half width, δ and wall shear velocity, u_τ. The computation is carried out with a non-dimensional time increment, $\Delta t = 0.002$, which maintained a CFL number [5, 6]:

$$CFL = \Delta t \max\left(\frac{|\langle \bar{u}_x \rangle|}{\Delta x} + \frac{|\langle \bar{u}_y \rangle|}{\Delta y} + \frac{|\langle \bar{u}_z \rangle|}{\Delta z}\right) = 0.334 < 1.0 \tag{4.1}$$

where, $\langle \bar{u}_i \rangle$ denotes an ensemble average of $\bar{u}_i$.

The computation is executed up to time, $t = n\Delta t$, where n is the number of time step. The computational domain is discretized with uniformly distributed grid in all the directions, and the grid spacing in the corresponding directions are $\Delta x^+ \approx 116$, $\Delta z^+ \approx 58$ and $\Delta y^+ \approx 59$ wall units respectively. The first mesh point away from the wall is at$y^+ \approx 29.5$wall unit. The superscript '+' indicates a non-dimensional quantity scaled by the wall variables; e.g., $y^+ = y u_\tau/\nu$, where ν is the kinematic viscosity and $u_\tau = (\tau_w/\rho)^{1/2}$ is the wall shear velocity.

5. BOUNDARY CONDITIONS

We consider fully developed incompressible viscous flow and make use of periodic boundary conditions in the streamwise and spanwise directions. For the staggered grid arrangement we set up additional nodes surrounding the physical boundary. The calculations are performed at internal nodes only. The wall boundary condition is no-slip. Just outside the solution domain the values of the velocity components are equated to the values of the nearest node just inside the solution domain [24]. The pressure boundary condition is periodic in the streamwise and spanwise directions. But in the wall normal direction the values of p, just outside the solution domain, are determined by assuming a zero gradient [25].

6. ALGEBRAIC WALL MODEL

To reduce the calculation cost of LES, the near wall layer is approximated by a special form of AWM given by Spalding [14]. In this model one uses Spalding's law as an algebraic equation to calculate the wall shear stresses. Spalding's law is a non-linear equation about the wall shear velocity u_τ, whose special form is

$$y^+ = f\left(u^+\right) = u^+ + A\left[\exp\left(\kappa\, u^+\right) - 1 - \left(\kappa\, u^+\right)/2 - \left(\kappa\, u^+\right)^3\Big/6 - \left(\kappa\, u^+\right)^4\Big/24\right] \quad (6.1)$$

where, $A = exp\,(-\kappa B) = 0.1108, \kappa = 0.4$ and $B = 5.5$. The exceptional feature of Spalding's equation is that it presents y^+ as a function of u^+ rather than u^+ as a function of y^+. Here y is the distance from the wall and $y^+ = y\, u_\tau/\nu$ is the non-dimensional wall unit. In this equation u is the instantaneous horizontal velocity and $u^+ = u/u_\tau$ is the non-dimensional velocity at the first off-wall computational cells. At the first off-wall computational cells the LES velocity, $\sqrt{\langle \bar{u}_x \rangle^2 + \langle \bar{u}_z \rangle^2}$ is substituted to u of Eq. (6.1). Then Eq. (6.1) is solved by iterative procedure based on the Newton method for the wall shear velocity, u_τ. After that the instantaneous wall shear stresses are calculated as follows:

$$\tau_{w,\,x\,/\rho} = \left(\nu\, y^+/u^+\right)\ \bar{u}_x/y\,, \quad \tau_{w,\,z\,/\rho} = \left(\nu\, y^+/u^+\right)\ \bar{u}_z/y \quad (6.2)$$

These wall shear stresses are then used for the wall boundary condition of velocity fields. It is to be mentioned that the Spalding's formulation for the law of the wall with values of constants, A and κ has an undisputed advantage that it satisfies no-slip condition at the wall. Near to wall region Spalding's law governs the flow.

7. RESULTS AND DISCUSSIONS

7.1. **Turbulence Statistics.** In this section we discuss some statistics of the computed flow field in 3D turbulent channel flow. The computed results are compared with the DNS data obtained by Moser *et al.* [2] and LES data using no wall model (LES-NWM) obtained by Uddin and Mallik [5]. For comparison, the DNS data of Moser *et al.* [2] is represented by a solid line, the LES data of Uddin and Mallik [5] is represented by a line with arrow sign and the computed results using algebraic wall model (LES-AWM) are indicated by a line with circle in the following figures of this section. Furthermore, in this section we provide a sample of

error generation for LES-NWM and LES-AWM approaches at some positions in mean velocity profile. In error calculation, the DNS data are considered as the true value. In this study LES simulations are initialized with a random solenoidal velocity field and integrated ahead in time with finite viscosity.

Numerous experiments have shown that the boundary layer in a plane turbulent channel flow can be divided into two parts: the inner or near wall region and the outer region. At the near wall region, the dynamics is dominated by the viscous effects. In the outer region, it controlled by the turbulence. Each of these regions is split into several layers, corresponding to different types of dynamics. In the case of canonical boundary layer, the near wall region can be largely subdivided into three layers. These three layers are the viscous sub-layer ($y^+ \leq 5$), buffer layer ($5 < y^+ \leq 30$) and logarithmic inertial layer ($y^+ > 30$; $y/\delta \ll 1$) [21]. The outer region includes the end of the logarithmic inertial region and wake region.

The profile of the mean velocity non-dimensioned by the wall-shear velocity corresponding to the lower half of the channel is shown in Figure 2, which is defined as

$$u_x^+ = \frac{\langle \bar{u}_x \rangle}{u_\tau} \tag{7.1}$$

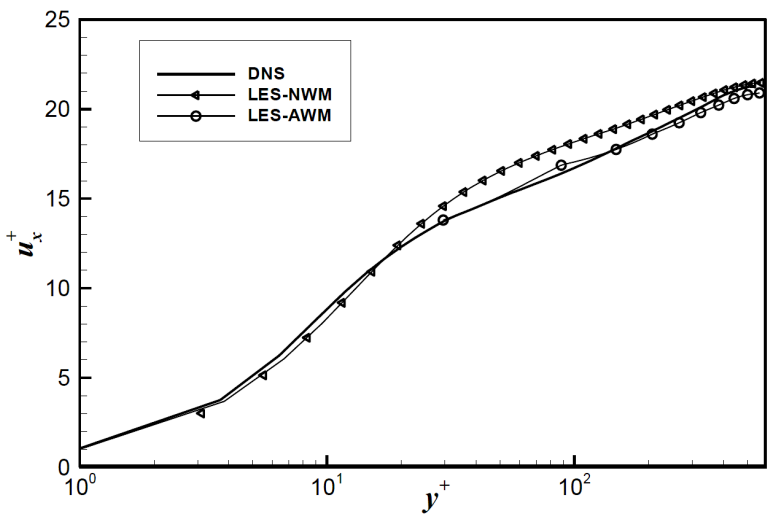

FIGURE 2. The mean velocity profile in wall units.

It can be observed that the computed profile cannot trace the data for the whole boundary layer. Here the first computational cell above the wall is located within the buffer layer ($5 < y^+ \leq 30$), at about $y^+ = 29.5$. That is, the AWM lead to a significant reduction in the number of computational cells at the near wall region. It has to be noted that our computed profile, LES-AWM under predicts the LES-NWM profile until end of the range. From this figure it is also revealed that the LES-AWM results are almost collapsed with the DNS results for $y^+ \approx 29.5 - 60$. Here after for $y^+ \approx 60 - 120$, the LES-AWM profile over predicts the DNS

profile. After that in rest of the range the LES-AWM profile under predicts the DNS profile. Nonetheless, Figure 3 shows that the agreement of the mean velocity profile for LES-AWM with the DNS data is better than that of the LES-NWM profile.

Errors generated in LES-NWM and LES-AWM approaches are presented in Table 1. From this table it can be observed that initially the percentage of relative error in LES-AWM approach is 1%. After that, upto a certain position the error in this approach increases with the increase of wall units. Then, the error decreases and at $y^+ \approx 147.50$ it becomes zero. After this position the error increases gradually with the increase of wall units. It is worth noting here that the errors generated in LES-AWM approach are smaller than that in the LES-NWM approach at maximum positions.

TABLE 1. Percentage of relative errors in mean velocity.

y^+	Error in LES-NWM	Error in LES-AWM
29.50	5.51%	1.00%
88.50	8.78%	2.80%
147.50	6.59%	0%
324.50	2.94%	1.04%
442.50	1.19%	1.71%

Figure 3(a, b, c) show the DNS and LES profiles of root mean square(r.m.s.) of velocity components normalized by the wall shear velocity defined as

$$u_{x\ r.m.s.}^{+} = \sqrt{\langle u_x^2 \rangle - \langle u_x \rangle^2} \Big/ u_\tau \tag{7.2}$$

$$u_{y\ r.m.s.}^{+} = \sqrt{\langle u_y^2 \rangle - \langle u_y \rangle^2} \Big/ u_\tau \tag{7.3}$$

$$u_{z\ r.m.s.}^{+} = \sqrt{\langle u_z^2 \rangle - \langle u_z \rangle^2} \Big/ u_\tau \tag{7.4}$$

Figure 3(a) reveals that above the wall the LES-AWM profile of streamwise root mean square velocity starts with 2.02 at $y^+ \approx 29.5$. At this position the value of the DNS and LES-NWM profiles are about 2.48 and 3.54 respectively. After this position the value of LES-AWM profile increases with the increase of wall units and attains the maximum value of about 2.50 at $y^+ \approx 88.5$. Where, the value of the DNS and LES-NWM profiles are respectively 1.79 and 2.29. Beyond $y^+ \approx 88.5$ the trend of LES-AWM profile is always decreasing like the pattern of DNS and LES-NWM profiles until end of the range. Although there exists a noticeable discrepancy from the DNS and LES-NWM profiles at the near wall region, but away from the wall the LES-AWM profile shows closer agreement with the DNS and LES-NWM profiles.

The profile of wall normal root mean square velocity in wall units is shown in Figure 3(b). From this figure it can be observed that initially from $y^+ \approx 59 - 120$, the LES-AWM profile under predicts the DNS profile, but over predicts the LES-NWM profile. Here after, from

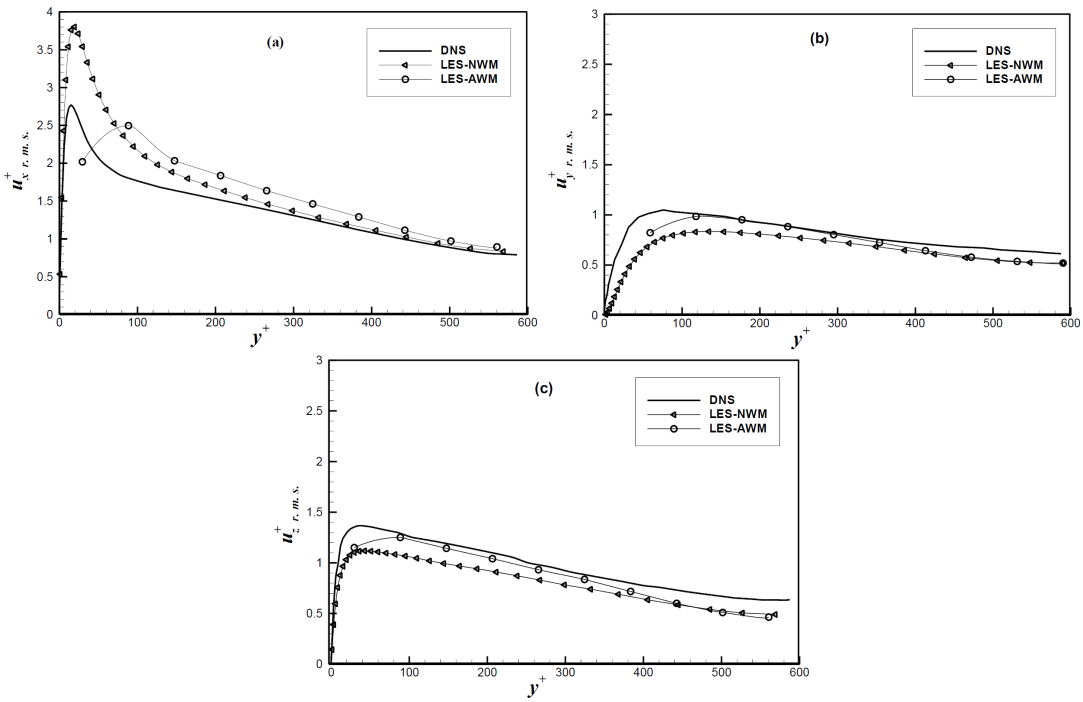

FIGURE 3. Root mean square velocity profiles in wall units.

$y^+ \approx 120 - 300$, there is hardly noticeable difference between the DNS and LES-AWM profiles. After that, in rest of the domain the LES-AWM profile under predicts the DNS profile. It has to be noted that, after a certain position the discrepancy between the LES-NWM and LES-AWM profiles decreases with the increase of wall units, and beyond $y^+ \approx 460$ the LES-NWM and LES-AWM profiles are almost collapsed. However, the profile of wall normal root mean square velocity for LES-AWM shows less discrepancy from the DNS profile than that of the LES-NWM profile.

The spanwise root mean square velocity profiles are displayed in Figure 3(c). This figure reveals that above the wall the LES-AWM profile starts with 1.15 near the peak value of LES-NWM profile at $y^+ \approx 29.5$. From this position the LES-AWM profile under predicts the DNS profile until end of the range and over predicts the LES-NWM profile up to $y^+ \approx 440$. Beyond $y^+ \approx 440$, in some of the regions ($y^+ \approx 120 - 300$) the LES-AWM and LES-NWM profiles are almost collapsed, and in rest of the range the LES-AWM profile under predicts the LES-NWM profile. However, in most of the region the LES-AWM profile shows closer agreement with the DNS profile than that of the LES-NWM profile.

The profile of non-dimensional Reynolds stress, $-\overline{u'_x\, u'_y}/u_\tau^2$ corresponding to the channel half width is shown in Figure 4. In a fully developed channel flow this profile is a straight line when the flow reaches an equilibrium state. Our computed results clearly indicate that this is

the case. This figure also reveals that the discrepancy of the LES-AWM profile with the DNS and LES-NWM profiles decreases with the increase of the value of y^+. Away from the wall ($y^+ > 400$), there is hardly noticeable difference between the three profiles.

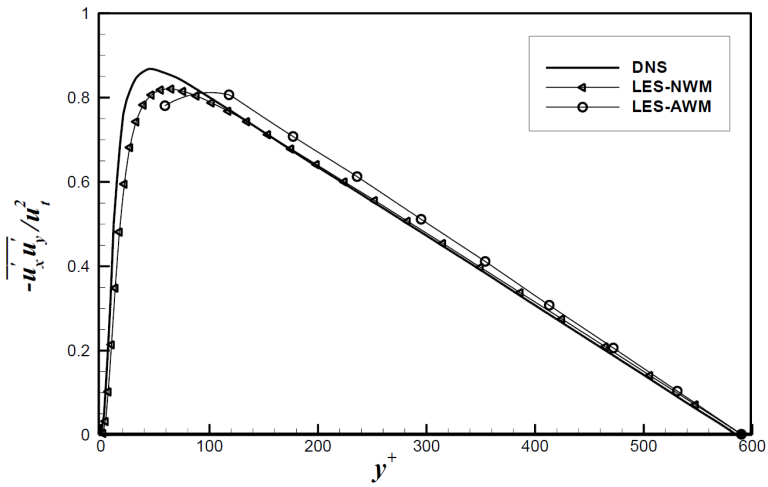

FIGURE 4. The Reynolds stress profile in wall coordinates.

7.2. **Flow Structures.** We have calculated streamwise velocity ($\bar{u}_x$) distribution at the centerline of the channel and streamwise shear velocity ($\bar{u}_{x\tau}$) distribution at the immediate vicinity of the wall at a non-dimensional time, $t = 202.20$ when the flow reaches to an equilibrium state. Using these computed data different contour plots of the flow field have been drawn and compared with the contours obtained by Uddin and Mallik [5].

Contour of instantaneous streamwise velocity distribution at the centerline of the channel in $x - z$ plane is shown in Figure 5(a), (b).

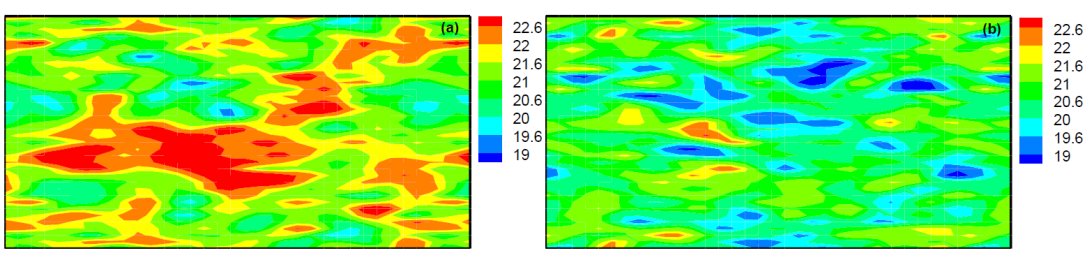

FIGURE 5. Contours of streamwise velocity profiles in $x - z$ plane for (a) LES using no wall model [5], and (b) LES using AWM.

Figure 5(a) is obtained by Uddin and Mallik [5], where no wall model has been used in LES, and in Figure 5(b), AWM has been used in LES. In these contour plots the value of $\bar{u}_x$ ranged

in between 19 and 22.6. The highest value of $\bar{u}_x$ is indicated by a red color, and the lowest value by a blue color. It has to be noted that in Figure 5(a) the higher values of $\bar{u}_x$ appear more densely adjacent to the centerline of the channel from both sides. But, in Figure 5(b) the higher values appear more densely in scattered locations of the $x-z$ plane. The distinctive features of the flow patterns in these contour plots are that the existence of high-speed fluid regions are more located in Figure 5(a) than that in Figure 5(b).

Contour of instantaneous streamwise shear velocity distribution at the immediate vicinity of the wall of this channel in $x-z$ plane is shown in Figure 6(a), (b).

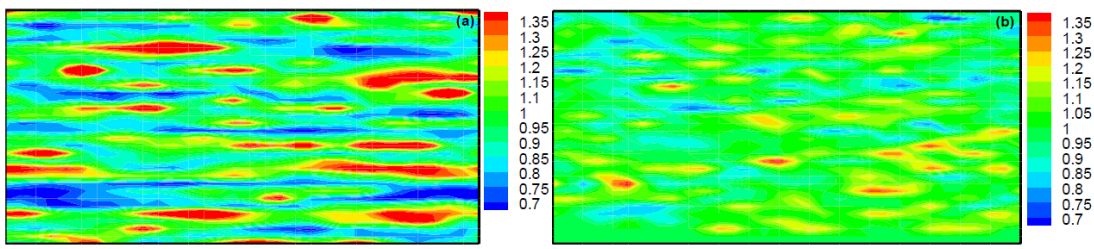

FIGURE 6. Contours of streamwise shear velocity profiles in $x-z$ plane for (a) LES using no wall model [5], and (b) LES using AWM.

In Figure 6(a) no wall model has been used in LES which is obtained by Uddin and Mallik [5], and in Figure 6(b), AWM has been used in LES. The value of $\bar{u}_{x\tau}$ ranged from 0.7 to 1.35 in these contour plots. The highest value appears at red regions and lowest value at blue regions. From these contour plots it can be observed that the regions of larger values of $\bar{u}_{x\tau}$ appear more densely in between the boundary and centerline of the channel. It is also noticeable that the intensity of $\bar{u}_{x\tau}$ in Figure 6(a) is higher than that located in Figure 6(b).

Figure 7(a), (b) represents the visualization of vortical structures in the turbulent channel flow by iso-surfaces of the second invariant Q of velocity gradient tensor, which is defined as [5, 6]:

$$Q = -\frac{1}{2}\left(S_{ij}\, S_{ij} - \Omega_{ij}\, \Omega_{ij} \right) \tag{7.5}$$

where,

$$S_{ij} = \frac{1}{2}\left(\frac{\partial \bar{u}_i}{\partial x_j} + \frac{\partial \bar{u}_j}{\partial x_i} \right) \quad \text{and} \quad \Omega_{ij} = \frac{1}{2}\left(\frac{\partial \bar{u}_i}{\partial x_j} - \frac{\partial \bar{u}_j}{\partial x_i} \right) \tag{7.6}$$

are respectively, the strain-rate and rotation tensors, that is, the symmetric and asymmetric part of the velocity gradient tensor:

$$A_{ij} = \frac{\partial\, \bar{u}_i}{\partial\, x_j} = S_{ij} + \Omega_{ij} \tag{7.7}$$

In Figure 7(a), no wall model has been used in LES which is obtained by Uddin and Mallik [5], but in Figure 7(b), AWM has been applied at the near wall region. The visualized region is the whole calculation domain. The level of the iso-surface is selected to be $Q = 5$. For this value of Q the vortical structures are significant and are randomly distributed over the

turbulent flow field. Generally, it can be noted that the vortices are generated in between near the boundary and the centerline of the channel are more intense than the ones are generated around the centerline of the channel. It is also noticeable that the vortices are generated more densely in Figure 7(a) than that of Figure 7(b).

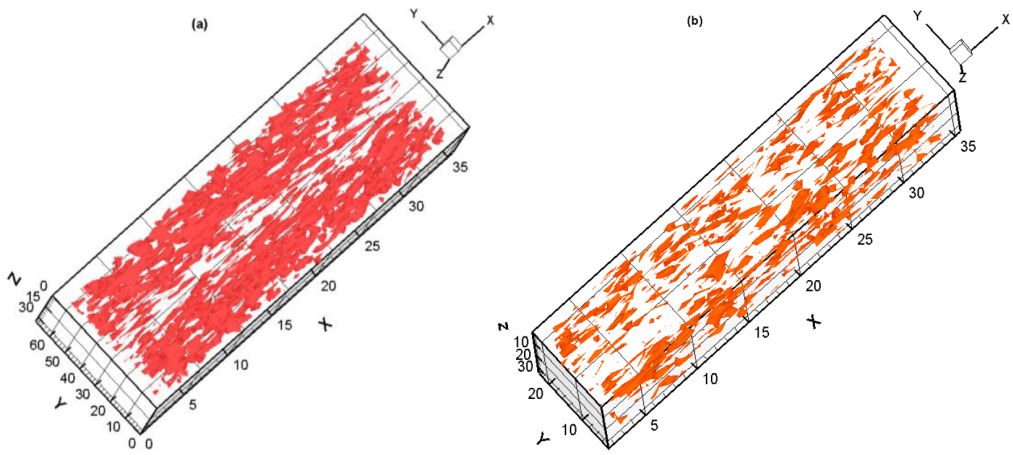

FIGURE 7. Iso-surfaces of the second invariant (Q =5) in the channel flow for (a) LES using no wall model [5], and (b) LES using AWM.

8. CONCLUSION

A Large eddy simulation of a turbulent channel flow has been successfully carried out using AWM at a Reynolds number, $Re_\tau = 590$ with $32 \times 20 \times 32$ grid points. To reduce the calculation cost, the AWM lead to a significant reduction in the number of computational cells at the near wall region. In spite of resolution limitations, the simulations are able to resolve the essential features of the statistical fields. The statistical results are compared with the DNS and LES data of reference. Maximum discrepancies are found at the near wall region. In comparison with the DNS data the computed results show better agreement than that of LES results using no wall model. Instantaneous streamwise velocity distribution at the centerline of the channel and streamwise shear velocity distribution at the immediate vicinity of the wall have also been measured in the contour plots, and compared these contour plots with those of LES data using no wall model. In our computation the higher values of streamwise velocity appear more densely in scattered locations of the centerline $x - z$ plane, and the higher values of streamwise shear velocity appear more densely in between the boundary and centerline of the channel. But the existence of high-speed fluid regions are less located in the computed flow field. Visualization of the iso-surfaces of the second invariant ($Q = 5$) in the turbulent channel flow show that the flow field contains lots of tube-like vortical structures which are randomly distributed over the turbulent flow field. The intensity of the vortical structures is

high in between near the boundary and the centerline of the channel. But the vortices are generated less densely in the computed flow field.

ACKNOWLEDGEMENTS

This research work is partially supported by the 'Bangabandhu Fellowship on Science and ICT Project' which is gratefully acknowledged. We also thank Dr. Jahrul Alam, Memorial University for his comments and suggestions for the improvement of this manuscript.

REFERENCES

[1] J. Kim, P. Moin, and R. Moser, *Turbulence statistics in fully developed channel flow at low Reynolds number*, Journal of Fluid Mechanics, **177** (1987), 133–166.

[2] R.D. Moser, J. Kim, and N.N. Mansour, *Direct numrical simulation of turbulent channel flow up to* $Re_\tau = 590$, Physics of Fluids, **11**(4) (1999), 943–945.

[3] P. Moin and J. Kim, *Numerical Investigation of Turbulent Channel Flow*, Journal of Fluid Mechanics, **118** (1982), 341–377.

[4] F. Yang, H.Q. Zhang, C.K. Chan, and X.L. Wang, *Large Eddy Simulation of Turbulent Channel Flow with 3D Roughness Using a Roughness Element Model*, Chinese Physics Letters, **25**(1) (2008), 191–194.

[5] M.A. Uddin and M.S.I. Mallik, *Large Eddy Simulation of Turbulent Channel Flow using Smagorinsky Model and Effects of Smagorinsky Constants*, British Journal of Mathematics & Computer Science, **7**(5) (2015), 375–390.

[6] M.S.I. Mallik, M.A. Uddin, and M.A. Meah, *Large Eddy Simulation of Turbulent Channel Flow at* $Re_\tau = 590$, IOSR – Journal of Mathematics, **10**(6) (2014), 41–50.

[7] Z. Xie, B. Lin, and R.A. Falconer, *Large-eddy simulation of the turbulent structure in compound open-channel flows*, Advances in Water Resources, **53** (2013), 66–75.

[8] G. GrÖtzbach, *Direct numerical and large eddy simulation of turbulent channel flows*. Encyclopedia of Fluid Mechanics, Cheremisinoff, N. P. ed., Gulf Pub. Co., Chap. 34, (1987), 1337–1391.

[9] H. Werner and H. Wengle, *Large eddy simulation of turbulent flow around a cube in a plane channel*, Selected Papers from the 8th Symposium on Turbulent Shear Flows, ed. F Durst, R Friedrich, BE Launder, U Schumann, JH Whitelaw, Springer, New York (1993).

[10] U. Piomelli and E. Balaras, *Wall-Layer Models for Large-Eddy Simulations*, Annual Review of Fluid Mechanics, **34** (2002), 349–374.

[11] G. Kalitzin, G. Medic, G. Iaccarino, and P. Durbin, *Near-wall behavior of RANS turbulence models and implications for wall functions*, Journal of Computational Physics, **204** (2005), 265–291.

[12] U. Schumann, *Subgrid scale model for finite difference simulations of turbulent flows in plane channels and annuli*, Journal of Computational Physics, **18** (1975), 376–404.

[13] U. Piomelli, J. Ferziger, P. Moin, and J. Kim, *New approximate boundary conditions for large-eddy simulations of wall-bounded flows*, Physics of Fluids, **1** (1989), 1061–1068.

[14] D.B. Spalding, *A single formula for the law of the wall*, Journal of Applied Mechanics, **28**, Ser. E (1961), 455–458.

[15] F.E. Ham, F.S. Lien, and A.B. Strong, *A Fully Conservative Second-Order Finite Difference Scheme for Incompressible Flow on Nonuniform Grids*, Journal of Computational Physics, **177** (2002), 117–133.

[16] Y. Morinishi, *Skew-symmetric form of convective terms and fully conservative finite difference schemes for variable density low-Mach number flows*, Journal of Computational Physics, **229** (2010), 276–300.

[17] Y.M. Han, J.S. Cho, and H.S. Kang, *Analysis of a one-dimensional fin using the analytic method and the finite difference method*, Journal of Korean Society for Industrial and Applied Mathematics, **9**(1) (2005), 91–98.

[18] M.Y. Kim and Y.K. Choi, *Efficient Numerical Methods for the KDV Equation*, Journal of Korean Society for Industrial and Applied Mathematics, **15**(4) (2011), 291–306.

[19] B. Sanderse and B. Koren, *Accuracy analysis of explicit Runge–Kutta methods applied to the incompressible Navier–Stokes equations*, Journal of Computational Physics, **231** (2012), 3041–3063.
[20] J.H. Williamson, *Low-storage Runge–Kutta schemes*, Journal of Computational Physics, **35** (1980), 48–56.
[21] P. Sagaut, *Large Eddy Simulation for Incompressible Flows: An Introduction*, Springer-Verlag, Berlin Heidelberg, (2001).
[22] C.A. Kennedy, M.H. Carpenter, and R.M. Lewis, *Low-storage, explicit Runge–Kutta schemes for the compressible Navier–Stokes equations*, Applied Numerical Mathematics, **35** (2000), 177–219.
[23] D.B. Johnson, P.E. Raad, and S. Chen, *Simulation of impacts of fluid free surfaces with solid boundaries*, International Journal for Numerical Methods in Fluids, **19** (1994), 153–176.
[24] H.K. Versteeg and W. Malalasekera, *An introduction to computational fluid dynamics*, Longman Group Limited, England, (1995).
[25] J.D. Anderson, *Computational Fluid Dynamics*, McGraw-Hill, New York, (1995).